INTERNATIONAL JOURNAL FOR NUMERICAL METHODS IN FLUIDS
Int. J. Numer. Meth. Fluids **26**: 697–712 (1998)

COMPUTATION OF VISCOELASTIC CABLE COATING FLOWS

I. MUTLU[1], P. TOWNSEND AND M.F. WEBSTER*

Institute of Non-Newtonian Fluid Mechanics, University of Wales, Singleton Park, Swansea, SA2 8PP, UK

SUMMARY

A viscoelastic analysis is presented for model tube tooling, draw-down and combined geometry flows encountered in the cable coating industries. The work investigates the development of stress fields and studies the effect of varying entry flow stress boundary conditions. The analysis takes into account tube tooling and draw-down flow sections individually, and in combination. The flow behaviour of cable-coating grade low density polyethylene is studied assuming a viscoelastic, isothermal flow, and employing a Taylor–Petrov–Galerkin finite element scheme with an exponential Phan-Thien–Tanner constitutive model. © 1998 John Wiley & Sons, Ltd.

KEY WORDS: viscoelastic; boundary conditions; tube tooling; cable-coating; finite elements

1. INTRODUCTION

The process of coating wide-bore cables consists of two flow regimes, namely a shear-dominated flow within the tube tooling or die region, and an extension-dominated flow in a draw-down region, where the melt meets the cable. The molten polymer is injected into the tooling die and flows under the influence of a pressure gradient. The extruded molten plastic tube makes contact with the cable beyond the die, where it is drawn out in the form of a sheath around the cable. The motion of the cable induces a drag flow. The coating process is a free-surface problem, by which a film of liquid is continuously deposited on a rigid moving cable. Coating lines for wide-bore cables are run at relatively low speeds of 0.1–0.5 m s^{-1}. Alternative pressure tooling die designs, used for narrow-bore cables, are operated at speeds approximately ten times greater. In this instance, the coating meets the cable within the die itself.

There are a number of assumptions and approximations associated with the numerical simulation of such problems. These include neglecting the effect of elasticity, e.g. Tucker [1], Han *et al.* [2,3], Pearson *et al.* [4,5], Carley *et al.* [6], Basu [7], Agur *et al.* [8], Mitsoulis *et al.* [9] and Binding *et al.* [10]; the assumption of isothermal flow, e.g. Han *et al.* [2,3], Caswell *et al.* [11] and Mitsoulis *et al.* [12]; the choice of boundary condition to be assigned at the melt–metal interface (Tucker [1]), where no-slip boundary conditions are usually employed (Arpin *et al.* [13] and Basu [7]); the selection of a suitable constitutive equation to describe the

* Correspondence to: Institute of Non-Newtonian Fluid Mechanics, University of Wales, Singleton Park, Swansea, SA2 8PP, UK.
[1] Present address: Middlesex University, Department of Mechanical Engineering, Bounds Green Road, London N11 2NQ, UK.

CCC 0271–2091/98/060697–16$17.50

Received March 1997
Revised June 1997

material behaviour (Pearson [5], Saramito *et al.* [14] and Mitsoulis [15]); and the approach in modelling the free surface flow in the draw-down section. Contact lines are either static attachment or separation lines, where a fluid intersects a stationary die surface, or dynamic wetting lines, where the polymer melt continually encounters new cable to be coated. A further complication is the location of free surfaces, and thus the start of the wetting line, which are unknown *a priori*. Some of the studies presume these positions are known (e.g. Gunter *et al.* [16]), others determine the position of the free surfaces iteratively (Agur *et al.* [8], Mitsoulis [17] and Heng *et al.* [18]). The present work concentrates on coatings with molten low density polyethylene (LDPE), assuming isothermal conditions, no-slip within the die, and a fixed location for the free surfaces. An exponential Phan-Thien–Tanner constitutive model is chosen to fit the steady shear and uniaxial extension data determined by Walters *et al.* [19].

This study naturally follows the precursor investigation of Gunter *et al.* [16], in which model extensional flows were analysed. This included a viscoelastic analysis for a number of test problems, culminating in a draw-down flow. Stress prehistory was absent from this earlier work. The objectives here are to study the sensitivity of the numerical results to adjustments in stress boundary conditions within the context of a single mode, viscoelastic analysis for isolated tube tooling, draw-down, and combined tube tooling–draw-down flows. This will cast some light on the influence of prehistory for the separate and combined flow subproblems. Segmentation of the flow into subproblems enables a systematic study, permitting isolation of the competing extension and shear effects associated with the various subsections of the problem.

2. GOVERNING EQUATIONS AND PROBLEM SPECIFICATION

The non-dimensional system of equations consists of the momentum equation,

$$Re\frac{\partial \boldsymbol{u}}{\partial t} = \nabla\cdot(2\mu_2\boldsymbol{D} + \tau) - Re\boldsymbol{u}\cdot\nabla\boldsymbol{u} - \nabla p, \tag{1}$$

the continuity equation,

$$\nabla\cdot\boldsymbol{u} = \boldsymbol{0}, \tag{2}$$

and the Phan-Thien–Tanner (PTT) constitutive equation,

$$We\frac{\partial \tau}{\partial t} = 2\mu_1\boldsymbol{D} - f\tau - We\{\boldsymbol{u}\cdot\nabla\tau - \nabla\boldsymbol{u}\cdot\tau - (\nabla\boldsymbol{u}\cdot\tau)^{\dagger} + \xi[\boldsymbol{D}\tau + (\boldsymbol{D}\tau)^{\dagger}]\}, \tag{3}$$

where $\boldsymbol{u}$ is the velocity vector, p is the isotropic pressure, τ is a polymeric extra-stress tensor, $\boldsymbol{D}$ is the rate of deformation tensor, t is the independent time variable, ∇ is the gradient operator and † denotes matrix transpose. For the exponential version of the PTT model, the non-linear function f is defined as,

$$f = \exp\left[We\frac{\varepsilon}{\mu_1}\,\mathrm{trace}(\tau)\right]. \tag{4}$$

Non-dimensionalisation requires scales of U for velocity (cable velocity), L_c for length (the length of the extension region of the draw-down flow), L_c/U for time, and $\mu\,(U/L_c)$ for stress and pressure. Here, μ is a zero-shear rate viscosity, given by $\mu = \mu_1 + \mu_2$, where μ_1 is a polymeric viscosity (that vanishes for a Newtonian fluid) and μ_2 is a solvent viscosity. Non-dimensional groups of Reynolds number and Weissenberg number are defined as $Re = \rho U L_c/\mu$ and $We = (U/L_c)\,\lambda_1$ respectively, where ρ is the fluid density and λ_1 is a relaxation time. PTT models (e.g. Bird *et al.* [20]) are referred to as PTT(ε, ξ), for which the constant viscosity Oldroyd-B model is given by PTT(0, 0). The parameters ε, ($\varepsilon \geq 0$) and ξ ($0 \leq \xi \leq 2$) are material parameters that govern the elongational and shear properties of the model, respectively. Models with $\varepsilon = 0$, demonstrate a constant shear viscosity for either $\xi = 0$ (Oldroyd-B model) or $\xi = 2$, and are shear thinning otherwise (Carew *et al.* [21]).

The solution of Equations (1)–(3), with appropriate boundary and initial conditions, is performed based on a Taylor–Petrov–Galerkin–pressure-correction finite element scheme of Carew *et al.* [21]. This involves a fractional-staged approach for solving velocity, stress and pressure as primary variables of the system, with a time stepping scheme to calculate stationary solutions for complex flows of viscoelastic fluids. Semi-implicitness is incorporated within the time stepping scheme for the momentum equation, whilst the constitutive equation is solved using an explicit procedure. Each fractional-staged equation is solved by an iterative solver, bar the pressure Poisson equation for which a direct Choleski method is used. A decoupled scheme variant, which linearises the problem by employing Newtonian kinematics as frozen coefficients for the viscoelastic problem (Carew *et al.* [22]), is invoked to obtain steady-state solutions. This analysis is efficient and stabilising to the solution process and yields a first estimate of stress fields. Also, it provides a route to access multi-mode predictions via an iterative combination of single-mode solutions.

Due to the highly elastic and convection-dominated nature of the constitutive equations, streamline upwinding, SUPG (Carew *et al.* [21]) is employed to suppress streamwise oscillations in the discrete solution. A high degree of accuracy is enforced via a Jacobi iteration, to suppress cross-stream oscillations (Gunter *et al.* [16]). At each fractional stage, seven Jacobi iterations are used for the isolated draw-down flow. Similarly, five iterations are employed for the isolated tube tooling die flow and the combined geometry flow. A Courant number stability constraint is used to determine the time step of 10^{-3} for all meshes and geometries. Detailed discussion on the numerical scheme and its implementation is provided elsewhere (Gunter *et al.* [16], Carew *et al.* [21,22]), and for brevity is not repeated here.

To complete the problem specification it is necessary to prescribe initial and boundary conditions. For all problems considered, geometries are annular in cross-section, requiring an axisymmetric frame of reference, and simulations are conducted at a fixed Reynolds number of 2.78×10^{-4}. The melt flow is assumed to be incompressible and isothermal, with material properties corresponding to a coating grade for LDPE. In non-dimensional form, the parameters used are: $\mu_1 = 0.9995$, $\mu_2 = 0.0005$, $\varepsilon = 0.1$ and $\xi = 0.01$. These parameters are taken from a fit of the PTT model to steady simple shear and uniaxial extension rheometrical data of Walters *et al.* [19]. In practice, a spectrum of relaxation times is associated with each material. To a first approximation, a single-mode analysis is conducted and results are reported for $0.1 \leq We \leq 28$. For all We number simulations, initial conditions are taken as frozen Newtonian kinematics with relaxed stress. The following nomenclature identifies the various entry flow boundary condition combinations that are considered:

BC1: Newtonian pressure-driven annular shear flow with PTT(0, 0.01) stress;

BC2: Newtonian pressure-driven annular shear flow with PTT(0.1, 0.01) stress;
BC3: Plug flow with uniaxial-extension PTT(0.1, 0.01) stress;
BC4: Plug flow with relaxed (zero) stress.

The first two cases are shear flow alternatives, with option BC1 providing algebraic simplicity for ease of practical implementation, whilst BC2 gives consistency with the interior flow. The last two cases are appropriate for extensional flow, as there is an absence of prehistory in option BC4, and BC3 matches the internal flow conditions.

2.1. Tube tooling flow

A schematic diagram of the tube tooling geometry and associated finite element grid is shown in Figure 1. Empirical investigation with coarser and finer grids led to this choice on the grounds of accuracy and efficiency. The fluid enters the geometry at AL with a fully developed pressure-driven Newtonian annular velocity profile, $V_i(r)$ (Bird *et al.* [23]), and exits at DI with profile, $V_o(r)$, likewise R_i and R_o in Figure 1 are the inner and outer radii, respectively. No-slip boundary conditions are imposed along the die walls, AD and IL. Vanishing pressure datum and radial velocity also apply on the domain outlet. Inlet boundary conditions for stress are determined analytically under the assumption of a fully developed simple shear flow and the PTT(ε, ξ) model satisfying Equation (3). For a shear rate $\dot{\gamma}(r)$, such boundary conditions are given by,

$$\tau_{rz} = (\mu_1 \dot{\gamma} f)/[f^2 + We^2(\dot{\gamma})^2 \xi(2-\xi)], \tag{5a}$$

$$\tau_{rr} = -(We\xi\dot{\gamma}\tau_{rz})/f, \tag{5b}$$

$$\tau_{zz} = -[We(2-\xi)\dot{\gamma}\tau_{rz}]/f, \tag{5c}$$

and

$$\tau_{\theta\theta} = 0. \tag{5d}$$

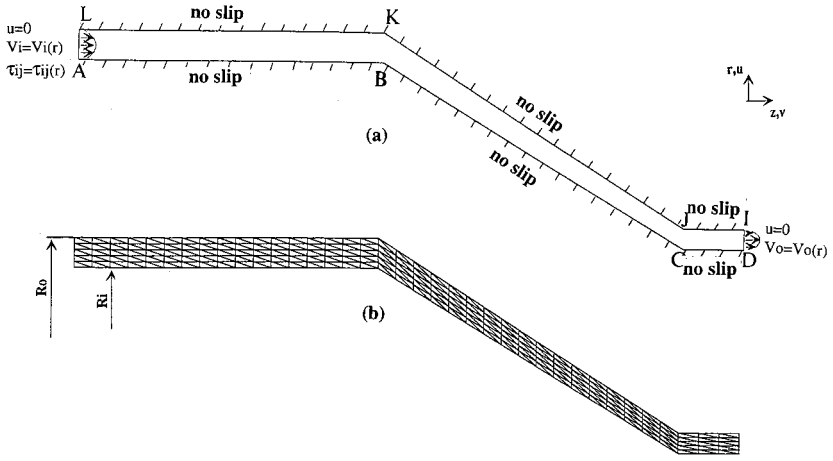

Figure 1. Tube tooling flow: (a) computational geometry and (b) finite element grid.

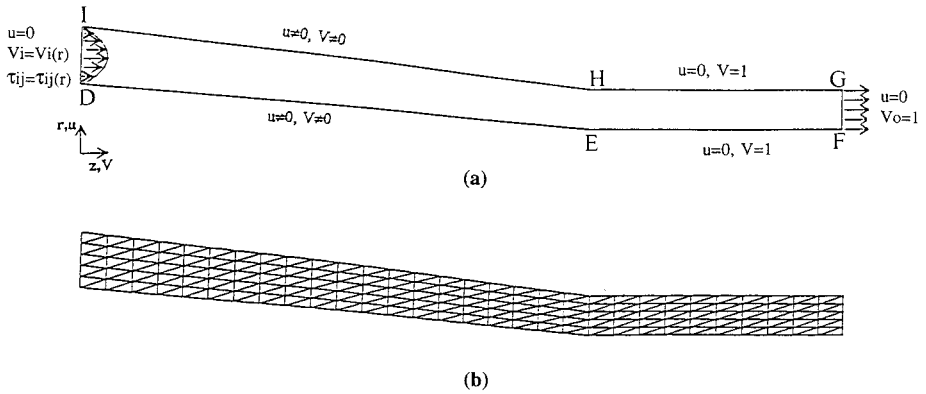

Figure 2. Draw-down flow: (a) computational geometry and (b) finite element grid.

Note, that the parameter f in the above equations is unity for a PTT(0, ξ) model. Alternatively, for a PTT(ε, ξ) model, f satisfies

$$\ln f = [2\varepsilon(We\dot{\gamma})^2(1-\xi)]/[f^2 + (We\dot{\gamma})^2\xi(2-\xi)]. \tag{5e}$$

A Newton iteration is employed to determine f from relationship (5e).

2.2. Isolated draw-down flow

The draw-down geometry, together with the mesh employed is illustrated in Figure 2. At the inlet boundary DI (Figure 2) option BC1 is analysed first, with PTT(0, 0.01) stress for the exit flow profile from the tube tooling die, as specified above. Boundary conditions over the remainder of the domain are as follows: along the traction-free surfaces (DE and GI in Figure 2) the velocity is defined as the resultant velocity approximated from the condition of constant melt flow rate. Vanishing radial velocity and pressure datum, together with a plug-like velocity profile, are specified at the exit boundary, GF. The boundary EF is assumed to move with the cable. The assumption of a simple shear flow at the inlet of the draw-down geometry with stress values calculated using a PTT(0, 0.01) model, is inconsistent with the interior solution generated for a PTT(0.1, 0.01) version. A growth in τ_{zz} stress caused by the dragging action of the cable is anticipated in the draw-down cone, together with a subsequent stress relaxation as the fluid travels in contact with the cable. Imposing BC1 option inlet stress conditions results in relatively high entry stress levels, thus causing some unexpected results.

For this subproblem and consistency, it is more appropriate to match the inlet stress conditions to the type of flow generated within the draw-down, being an extension-dominated flow. To this end, a uniaxial extensional entry flow with a plug-like velocity profile is also tested (option BC3). Using a constant and uniform extension rate, $\dot{\varepsilon}_{\text{in}}$ at the inlet, fully developed PTT(ε, ξ) stress values are computed viz:

$$\tau_{zz} = 2\mu_1\dot{\varepsilon}_{\text{in}}/[f - 2We\dot{\varepsilon}_{\text{in}}(1-\xi)], \tag{6a}$$

$$\tau_{rr} = \tau_{\theta\theta} = -\mu_1\dot{\varepsilon}_{\text{in}}/[f + We\dot{\varepsilon}_{\text{in}}(1-\xi)], \tag{6b}$$

and

$$\tau_{rz} = 0, \tag{6c}$$

where f satisfies the relationship,

$$\ln f = [6(We\dot{\varepsilon}_{\text{in}})^2\varepsilon(1-\xi)]/\{[f - 2We\dot{\varepsilon}_{\text{in}}(1-\xi)][f + We\dot{\varepsilon}_{\text{in}}(1-\xi)]\}. \tag{7}$$

A suitable non-dimensional inflow extension rate, $\dot{\varepsilon}_{in}$, is taken as $\dot{\varepsilon}_{in} = \Delta V/\Delta Z$, being a simple approximation over the first few mesh elements.

2.3. Combined tube tooling–draw-down flow

This flow comprises of the two individual flow sections described above, merged to form a single domain. A schematic diagram of the combined geometry together with notation, boundary conditions and its associated finite element grid is provided in Figure 3. The imposed boundary conditions are a combination of those reported for the isolated tube tooling flow and draw-down geometry flow. The only exception here is that now there is no disjunction in the flow at the end of the tube tooling die and the start of the draw-down flow. The solution will provide a check on the localised stress conditions that pertain to the join of the two subproblems, and an indication of their discrepancy from the idealised boundary conditions otherwise imposed.

3. RESULTS AND DISCUSSION

3.1. Tube tooling flow

The variation in the magnitude of velocity along various sample flow lines indicates that fully developed flow is established over the entry section of the tube tooling die, followed by an increase at the converging section. In the outlet section, the numerical results coincide almost exactly with the imposed analytical boundary condition.

It is more straightforward algebraically to specify boundary conditions with models for which $\varepsilon = 0$ and $f = 1$. The influence on solution development of consequent perturbation in the boundary condition becomes a point at issue once $\varepsilon > 0$ and f is non-constant. Preliminary solutions at $We = 0.1$ and 1 for the isolated tube tooling geometry with an annular velocity profile and PTT(0, 0.01) stress (option BC1) have shown that, immediately after entering the tube tooling geometry, τ_{zz} stress experiences spatial oscillations, which die out as the flow progresses through the geometry. These streamwise oscillations at entry are due to the nature of the imposed inlet stress boundary conditions, being inconsistent with the PTT(0.1, 0.01) model used to simulate the interior flow. Nevertheless, the entry section of the tube tooling geometry is long enough for the stress to reach a fully developed state before the flow enters the converging section. Hence at low We and for such a long hydrodynamic development section, the problem is relatively insensitive to perturbations in the inlet stress boundary condition; however, spatial oscillations begin to appear with increasing We. These oscillations are eliminated by imposing a fully developed flow with an annular velocity profile and consistent PTT(0.1, 0.01) stress at the inlet (option BC2). In Figure 4, axial profiles of τ_{zz} stress are presented for the tube tooling geometry with BC2-type stress boundary conditions for $0.1 \leq We \leq 15$, along sample lines at two radial locations, R4 and R5 (taken with respect to the exit of the tube tooling geometry, as indicated in Figure 4(a)). Although there is a difference between values at different radial locations, common to all plots, the stress field is fully developed within the inlet section of the tube tooling geometry, as expected. There is a stress build-up at the converging section, the growth rate being larger for $We < 1$, a result in agreement with the findings of Gunter *et al.* [16]. Figure 4 reveals that τ_{zz} stress is larger nearer the inner die wall (R5 over R4), and that there is some stress relaxation at the land region exit section (CD). Note also, that oscillations are particularly prominent for $We \leq 1$ at the entry, C, and exit, D, of the land region. Such sharp oscillations necessitate mesh refinement to reflect

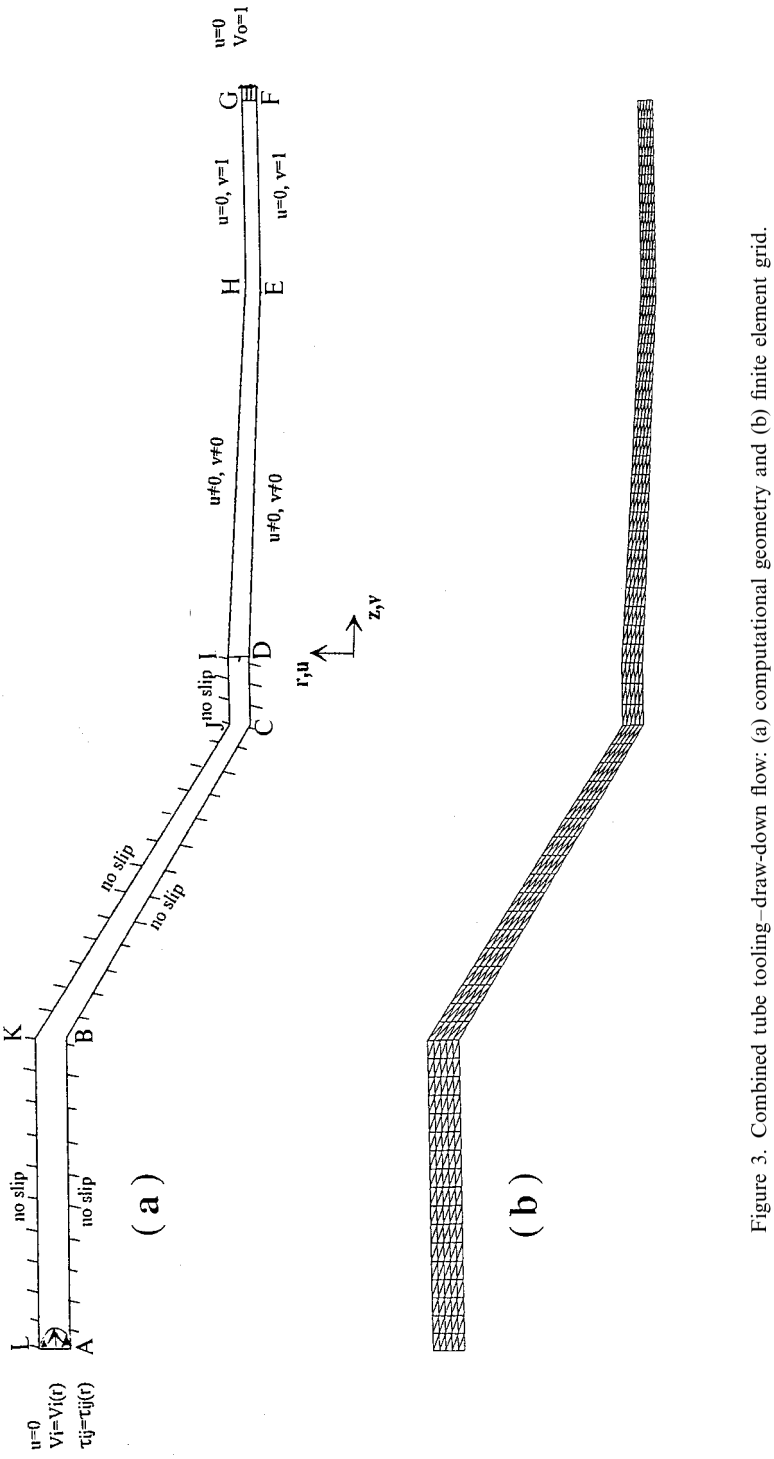

Figure 3. Combined tube tooling–draw-down flow: (a) computational geometry and (b) finite element grid.

smooth transition and are captured more accurately through adaptive remeshing, results for which are presented elsewhere (Mutlu *et al.* [24]).

The flow in the tooling is initially shear dominated, though both shear and extension interact through the converging section and the land region. Shear stress at the die outlet (CD) is depicted in Figure 5 for $0.1 \leq We \leq 15$ at four radial locations as above, maxima occurring at the inner die wall (R5). Stress build-up in this zone is critical to the process design. It is noted that the normal stress level is as much as five times larger than the shear stress level. Figure 5 reveals an increase in τ_{rz}, immediately after the melt enters the land section, at C, with subsequent stress relaxation. The τ_{rz} values for $We \geq 5$ essentially merge, and are almost constant along the radial and axial directions.

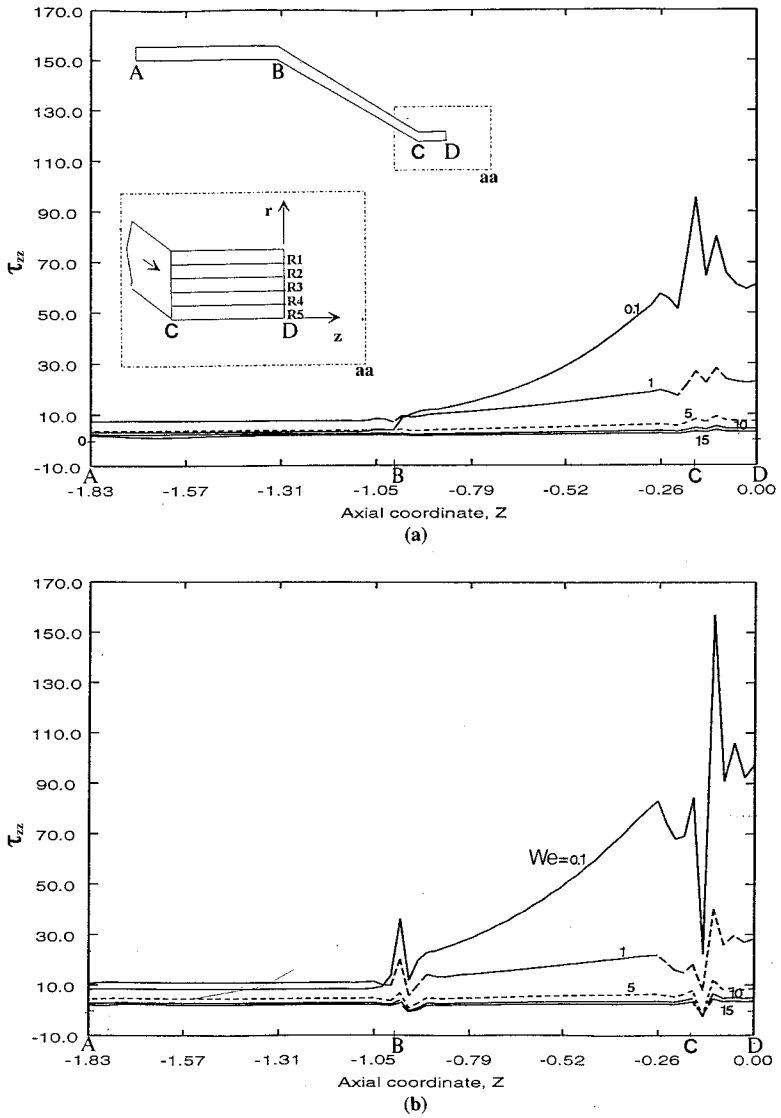

Figure 4. Tube tooling flow: axial profiles of τ_{zz} stress along two sample lines; (a) R4 and (b) R5; BC2 option.

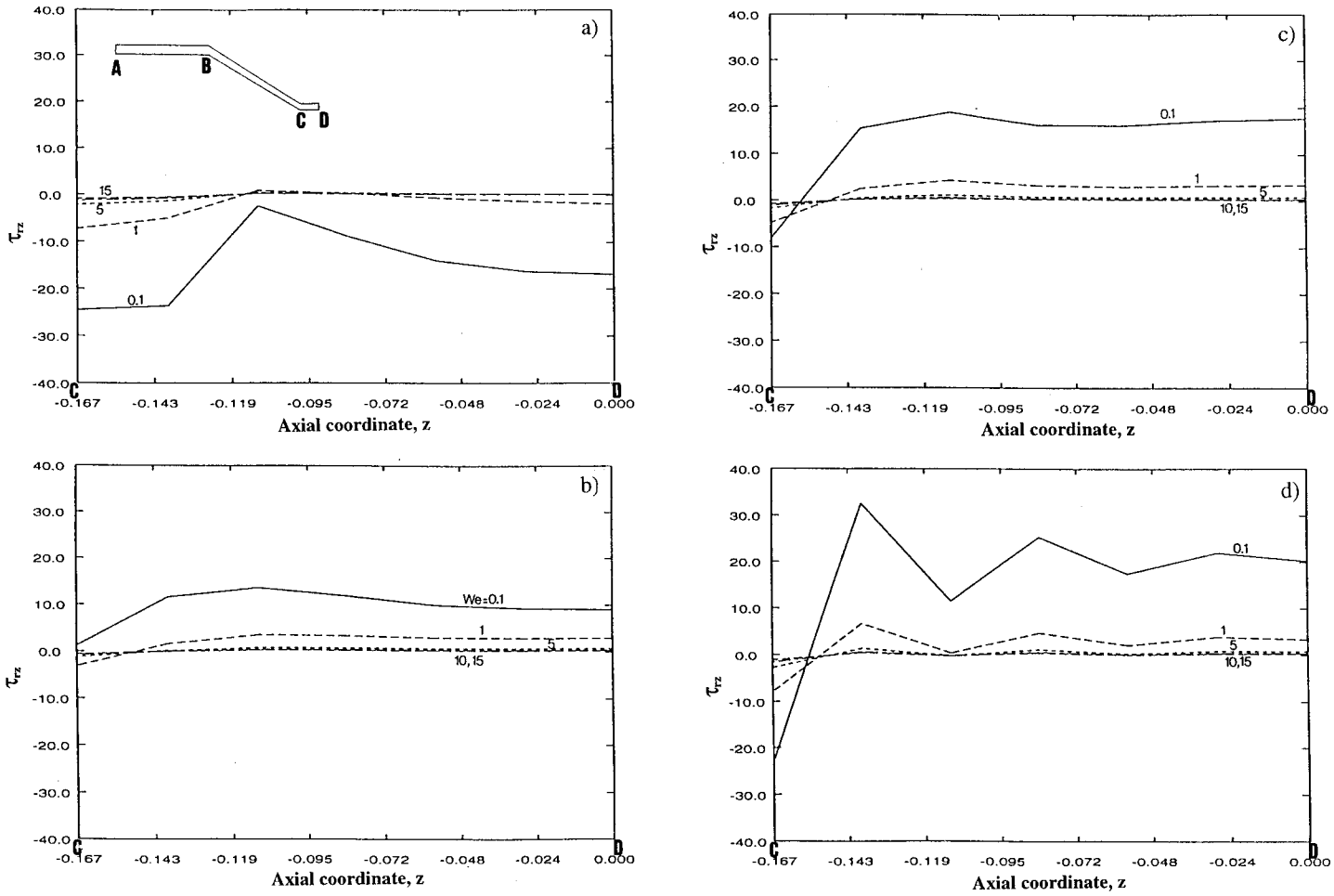

Figure 5. Tube tooling flow: axial profiles of τ_{rz} stress along four sample lines; (a) R1, (b) R3, (c) R4 and (d) R5; BC2 option.

With the present grids the range of convergence in We parameter space for the isolated draw-down and tube tooling flows is found to be significantly different. Experience has shown that solutions are attainable for the isolated draw-down flow up to $We = 28$, with some careful treatment (see Gunter *et al.* [16]). For the tube tooling flow, convergence is limited to $We = 15$. This points to the fact that once the predominantly extension-dominated draw-down flow has been resolved numerically, the greater complexity to the overall problem lies in solving the tube tooling part of the flow due to its inherent nature.

3.2. Draw-down flow

Commencing from an annular velocity profile at the inlet, DI, a plug-like flow is rapidly attained within 3% of the inlet tube length DE. An increase in velocity is observed in the draw-down cone ($0 \leq z \leq 1$), and the flow in contact with the moving wire ($1 \leq z \leq 1.5$) is fully developed. This velocity field is common to all We number tests for draw-down flow.

The variation in τ_{zz} stress for $0.1 \leq We \leq 28$ is shown in Figure 6 with BC1-type, Figure 7 with BC4-type, and Figure 8 with BC3-type boundary conditions. To facilitate direct comparison, the results reported in Gunter *et al.* [16] for option BC4 with relaxed inlet stress are reproduced in Figure 7. There is stress growth in the draw-down cone and relaxation within the flow on the cable. An increasing value of We retards stress growth. The observed stress growth in Figure 7, is almost entirely absent in Figure 6, except at $We = 5$. For option BC1 of Figure 6, the inconsistent inlet stress rearranges itself immediately, with longer readjustment lengths corresponding to lower We numbers. Within the extension region, the rise in τ_{zz} generates peak values prior to the impact region with the wire ($z = 1$). This differs from the instance in Figure 7, where a maximum is reached at the attachment point. For any given We value, stress maxima are larger for the instance with inlet PTT(0, 0.01) stress imposed than with PTT(0.1, 0.01) stress. Negative, unphysical τ_{zz} values are observed in Figure 6 for $We = 1$ and 5 with BC1 type boundary condition.

The assumption of a uniaxial extensional flow at a constant extension rate, consistent with the imposed plug-type velocity profile at the inlet of the draw-down flow (option BC3), is made to avoid these unphysical solutions. Predictions with these boundary conditions are depicted in Figure 8, displaying a τ_{zz} stress build-up in the draw-down cone, with maxima reached at the

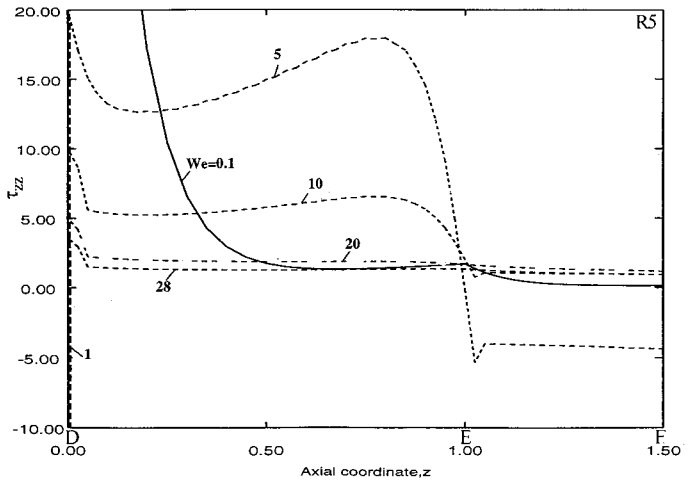

Figure 6. Draw-down flow: axial profiles of τ_{zz} stress; BC1 option.

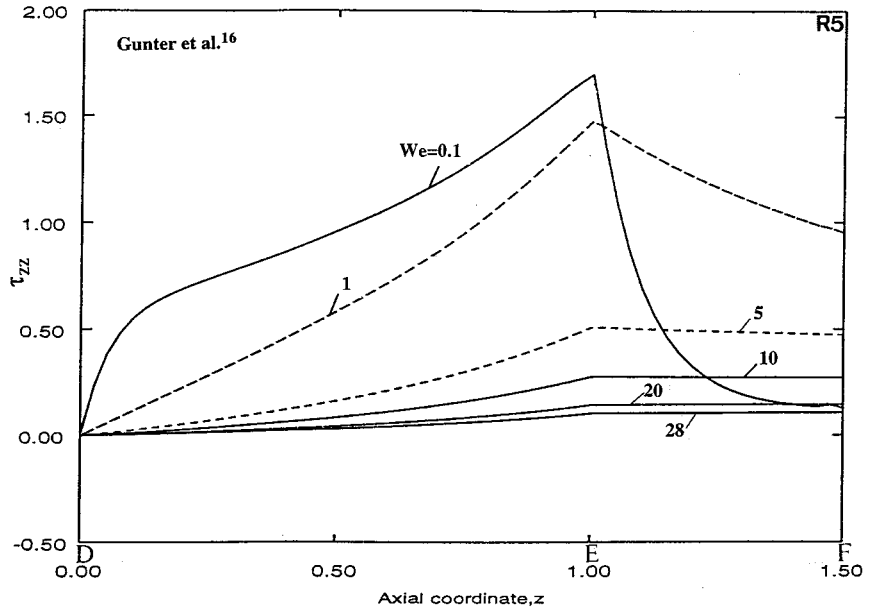

Figure 7. Draw-down flow: axial profiles of τ_{zz} stress; BC4 option.

same location as for relaxed inlet stress, and relaxation experienced in the flow on the cable. The trends in Figure 8 at any axial location reveal that τ_{zz} first increases in value as We increases from 0.1 to 5, reaches a maximum at $We = 5$, and then decreases as We is increased from 5 to 28. In contrast, with relaxed inlet stresses of Figure 7, the value of τ_{zz} decreases as We increases. The solutions of Figure 8 can be explained through the behaviour of the elongational viscosity as a function of $\lambda_1\dot{\varepsilon}$; first increasing with $\lambda_1\dot{\varepsilon}$ (extension thickening),

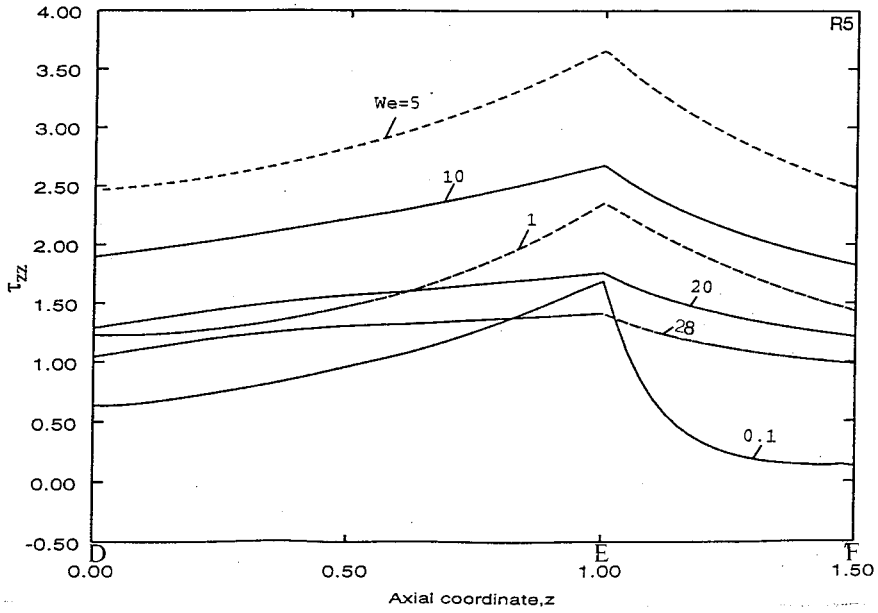

Figure 8. Draw-down flow: axial profiles of τ_{zz} stress; BC3 option.

reaching a maximum, and then decreasing (extension thinning). The assumption of a constant extension rate, $\dot{\varepsilon}$, implies that the extensional viscosity and, thus τ_{zz}, will first increase and then decrease as λ_1 (i.e. We) is increased. Although the velocity boundary condition at the entrance varies for the plots in Figures 6–8, the velocity field internal to the flow is virtually identical for the three cases. Hence, the difference in stress solution is attributable to the variation in inlet stress profile. The maximum values of τ_{zz} for $We = 0.1$ are almost identical, indicating that for low We, the resultant stress on the cable does not vary with the choice of boundary condition. This, however, is not the case for larger We values beyond unity. Resultant τ_{zz} stress on the cable is larger for option BC3 than BC4. Hence at higher We values, a stressed fluid state at the inlet, will result in larger stress on the cable than those for a relaxed inflow.

With options BC3 and BC4 for $We > 1$, there is no significant difference between τ_{zz} at various radial locations; for $We \leq 0.1$ and at the end of the domain, values are larger on the cable than internally. In contrast, for the case with an annular velocity profile and PTT(0, 0.01) inlet stress (option BC1), τ_{zz} varies radially in addition to the reported axial variation.

3.3. Combined geometry flow

For the combined flow problem, axial profiles of τ_{zz} stress along sample lines at four radial locations are shown in Figure 9 for $0.1 \leq We \leq 15$ and option BC2. R5 is the position of the sample line on the cable. With this single-mode analysis, no marked stress build-up is detected within the coating. At a detailed view, the general pattern is one of fully developed τ_{zz} stress at the inlet section of the tube tooling die, increase along its converging section, decrease at the end of the die tube ($z = 0$) and start of the draw-down section, growth along the draw-down cone (see insets in Figure 9), and finally decay within the coating flow ($1 \leq z \leq 1.5$). Relaxation at the die exit and start of the draw-down sections is most pronounced at $We = 0.1$. This is in agreement with the fact that for a purely viscous material ($We = 0$), the stress vanishes immediately after the strain is removed. Stress growth rate in the draw-down section is much reduced over that in the tube tooling die section.

Figure 10 presents a comparison of τ_{zz} results along a sample line of R5 for the isolated draw-down flow and combined geometry flow, with various inlet boundary conditions at $We = 0.1$ and 10. It is apparent that, for the isolated draw-down flow, different boundary conditions do not influence the resultant residual stress in the coating for $We \leq 0.1$. When We is increased, however, the use of uniaxial-extension PTT(0.1, 0.01) stress, as a boundary condition to the isolated draw-down flow (option BC3), slightly overpredicts the τ_{zz} stress in the flow on the cable. Nevertheless, option BC3 provides the closest match to the combined flow results. At the inlet of the isolated draw-down flow, the stress values resulting from BC1 type boundary condition are larger than those corresponding to the combined geometry flow with BC2 type inlet boundary conditions. It takes a considerable axial distance for these large draw-down inlet stresses to relax, before the start of the stress build-up in the draw-down cone. At $We = 0.1$, this distance is shorter for the combined geometry flow. The rate of decay of the draw-down inlet stress depends on initial values, with the rate being larger for lower inlet stress values. For τ_{rz} with consistent or inconsistent inlet stresses, an insignificant difference is observed in the coating flow for either the combined flow or the draw-down flow. An observation is that the level of the shear stress, built-up in the tube tooling die section, can be as large as one-third of the tensile stress.

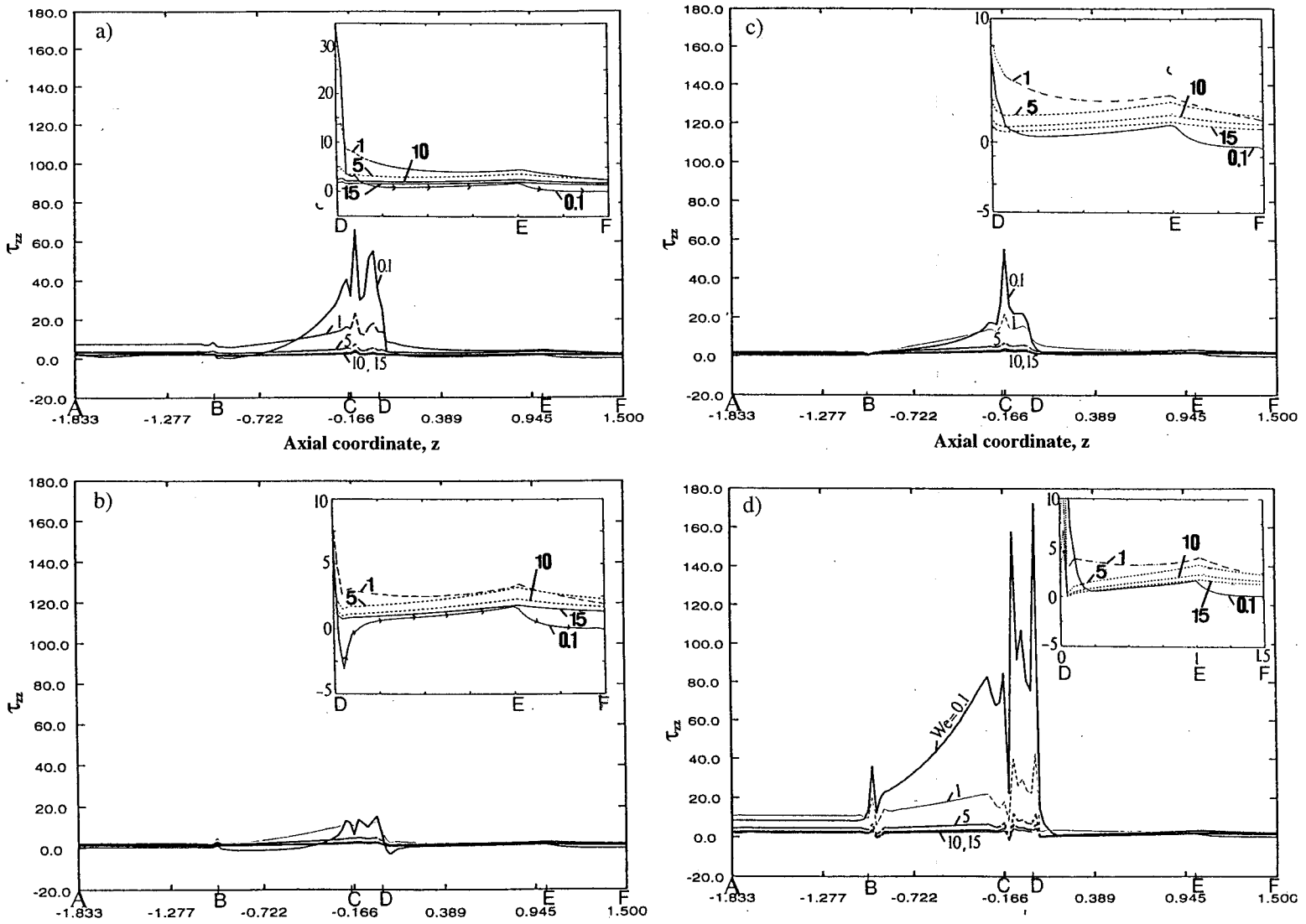

Figure 9. Combined tube tooling–draw-down flow: axial profiles of τ_{zz} stress along four sample lines; (a) R1, (b) R2, (c) R3 and (d) R5; BC2 option.

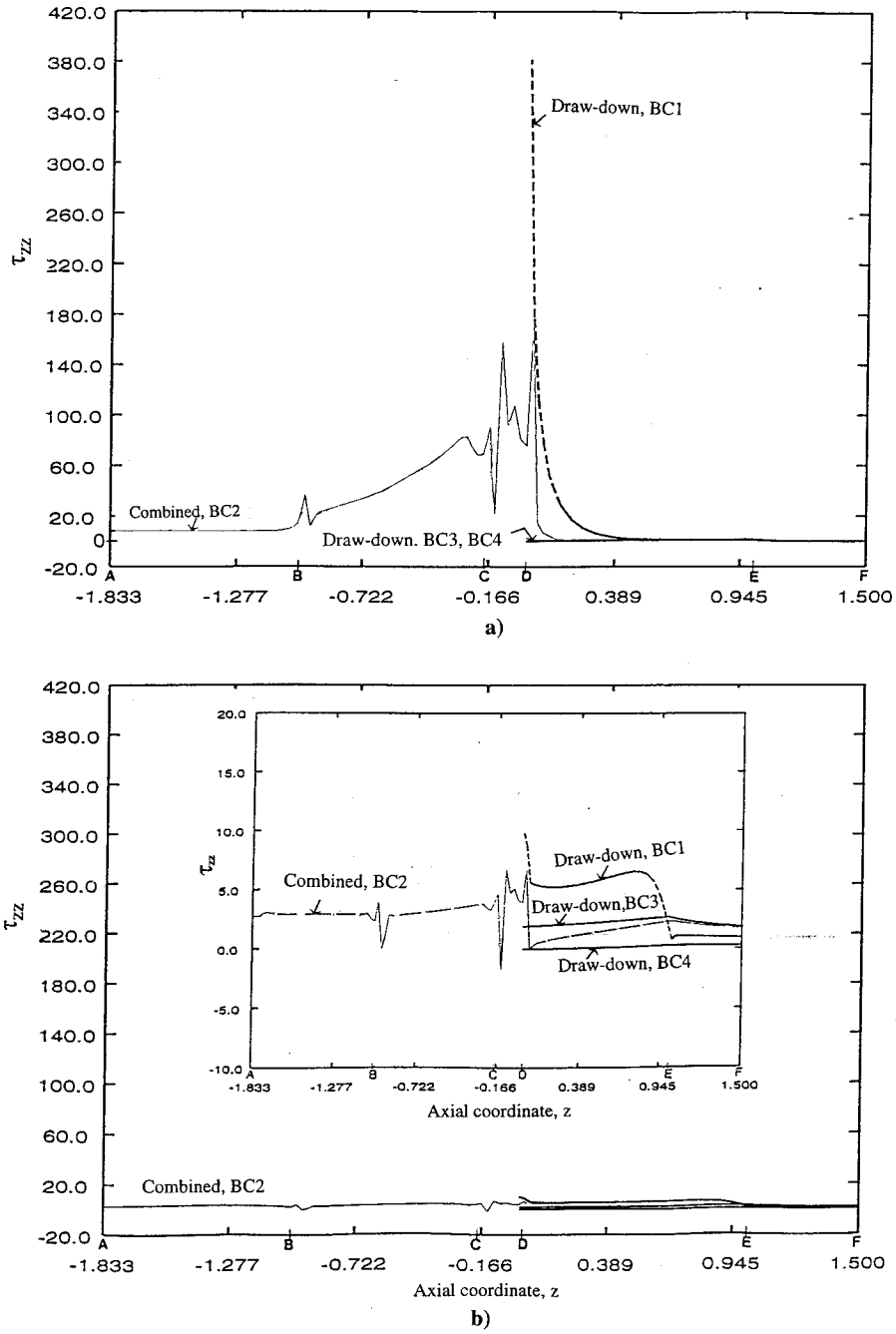

Figure 10. Combined tube tooling–draw-down and isolated draw-down flows: axial profiles of τ_{zz} stress; (a) $We = 0.1$ and (b) $We = 10$.

4. CONCLUSIONS

This paper has successfully demonstrated a viscoelastic analysis for tube tooling cable coating, a processing problem of industrial relevance. Under a single-mode approximation, there is barely any stress build-up detected within the coating. There is clearly a need to investigate this issue within a multi-mode context, which is the subject of an extended study. The results confirm that stresses are not fully relaxed at the die exit and entry to the draw-down section within the combined geometry flow. The imposition of arbitrary inlet stresses, inconsistent with the actual constitutive model employed at the interior of the domain, results in large stress values at the inlet of the isolated tube tooling flow and draw-down flow problems.

For the isolated draw-down flow, the use of various boundary conditions at the inlet reflects the sensitivity of the problem to boundary condition perturbation. These are not found to significantly affect the resultant stress values in the coating on the cable at low Weissenberg numbers. However, this is not the case as the level of Weissenberg number is increased. The assumption of a consistent uniaxial extension inlet flow, together with the analytically determined PTT stress, does have a considerable impact on these stress levels, yielding values close to those pertaining to the full combined geometry flow with marginal overprediction. On these grounds, the preferred choice of inlet boundary condition for isolated draw-down flow is option BC3, being superior to options BC1 and BC4, and providing the best match to the combined flow solution in the coating.

For the tube tooling flow, the use of inconsistent stresses at the inlet is not found to affect the overall solution, as the inlet annular section is sufficiently long for the stress to adjust to a fully developed state before reaching the converging section. This is also true for the combined geometry flow, proving insensitive to the boundary condition options tested. Hence, we have demonstrated that prehistory may be safely accommodated for this combined flow problem, adopting the techniques advocated. Prehistory is clearly a less significant issue to address for problems that commence from a shear-based flow, as opposed to those that emanate from an extensional flow.

ACKNOWLEDGMENTS

The authors wish to acknowledge the financial support and collaboration of BICC Cables within this study, and for the assistance provided in proof reading the final manuscript.

REFERENCES

1. C.L. Tucker, *Fundamentals of Computer Modelling for Polymer Processing*, Hanser, Oxford University Press, New York, 1989.
2. C.D. Han and D. Rao, 'Studies on wire coating extrusion. I. The rheology of wire coating extrusion', *Polymer Eng. Sci.*, **18**, 1019–1029 (1978).
3. C.D. Han and D.A. Rao, 'Studies on wire coating extrusion. II. The rheology of wire coating coextrusion', *Polymer Eng. Sci.*, **20**, 128–139 (1980).
4. J.R.A. Pearson and S.M. Richardson, *Computational Analysis of Polymer Processing*, Applied Science, London, 1983.
5. J.R.A. Pearson, *Mechanics of Polymer Processing*, Elsevier Applied Science, London, 1985.
6. J.F. Carley, T. Endo and W.B. Krantz, 'Realistic analysis of flow in wire-coating dies', *Polymer Eng. Sci.*, **19**, 1178–1187 (1979).
7. S. Basu, 'A theoretical analysis of non-isothermal flow in wire-coating coextrusion dies', *Polymer Eng. Sci.*, **21**, 1128–1138 (1981).
8. E.E. Agur and J. Vlachopoulos, 'Numerical simulation of a single-screw plastisizing extruder', *Polymer Eng. Sci.*, **22**, 1084–1094 (1982).

9. E. Mitsoulis, R. Wagner and F.L. Heng, 'Numerical simulation of wire-coating low-density polyethylene: theory and experiments', *Polymer Eng. Sci.*, **28**, 291–311 (1988).
10. D.M. Binding, A.R. Blythe, S. Gunter, A.A. Mosquera, P. Townsend and M.F. Webster, 'Modelling polymer melt flows in wirecoating processes', *J. Non-Newtonian Fluid Mech.*, **64**, 191–206 (1996).
11. B. Caswell and R.I. Tanner, 'Wirecoating die design using finite element methods', *Polymer Eng. Sci.*, **18**, 416–421 (1978).
12. E. Mitsoulis, J. Vlachopoulos and F. A. Mirza, 'Numerical simulation of entry and exit flows in slit dies', *Polymer Eng. Sci.*, **24**, 707–715 (1984).
13. B. Arpin, P.G. Lafleur and V. Lenir, 'Computer aided design of wire coating dies', *ANTEC '91*, 58–61, 1991.
14. P. Saramito, and J.M. Piau, 'Flow characteristics of viscoelastic fluids in an abrupt contraction by using numerical modelling', *J. Non-Newtonian Fluid Mech.*, **52**, 263–288 (1994).
15. E. Mitsoulis, 'Fluid flow and heat transfer in wire coating: A review', *Adv. Polymer Technol.*, **6**, 467–487 (1986).
16. S. Gunter, P. Townsend and M.F. Webster, 'The simulation of some model viscoelastic extensional flows', *Int. j. numer. methods fluids*, **23**, 691–710 (1996).
17. E. Mitsoulis, 'Finite element analysis of wire coating', *Polymer Eng. Sci.*, **26**, 171–186 (1986).
18. F.L. Heng and E. Mitsoulis, 'Numerical simulation of wire-coating coextrusion', *Intern. Polymer Processing IV*, 44–56 (1989).
19. K. Walters, D.M. Binding and R.E. Evans, 'Modelling the rheometric behaviour of 3 polyethylene melts', Internal Report, University of Wales, Aberystwyth, May 10, 1994.
20. R.B. Bird, R.C. Armstrong and O. Hassager, 'Dynamics of Polymeric Liquids', *Fluid Mechanics*, Vol. 1, 2nd Edn., Wiley, New York, 1987.
21. E.O. Carew, P. Townsend and M.F. Webster, 'A Taylor–Petrov–Galerkin algorithm for viscoelastic flow', *J. Non-Newtonian Fluid Mech.*, **50**, 253–287 (1993).
22. E.O. Carew, P. Townsend and M.F. Webster, 'Taylor–Galerkin algorithms for viscoelastic flow: application to a model problem', *J. Numer. Meth. Partial Differential Equations*, **10**, 171–190 (1994).
23. B. Bird, W.E. Stewart and E.N. Lightfoot, *Transport Phenomena*, Wiley, New York, 1960.
24. I. Mutlu, P. Townsend and M.F. Webster, 'Adaptive solutions for viscoelastic flows', *Comm. Numer. Methods Eng.*, **12**, 643–655 (1996).

